CHAPTER 6

SODIUM CONTAINING MULTICOMPONENT MESOPOROUS BIOACTIVE GLASSES: SYNTHESIS, CHARACTERIZATION AND IN-VITRO BIOACTIVITY

6.1 INTRODUCTION

Bioactive glasses (BGs) and glass-ceramics are mainly silica based, surface active bone substitutes, which shows good biocompatibility with the bone and soft tissues. Due to this remarkable property, these materials have been used in variety of biomedical applications, such as implants in clinical bone repair and as regeneration materials, coating-materials in tissue engineering, drug delivery, etc. [1-3]. One of the pre-requisite for the glass and glass-ceramics to bond and to integrate with living bone is the formation of a layer of biologically active hydroxycarbonate apatite (HCA) on the surface, when they are exposed to physiological fluids. In this context, significant effort has been made for developing various glass and glass-ceramic compositions with the improved bioactive properties [4-6]. It has been observed that the HCA formation is strongly influenced by chemical composition, structure and textural properties of glass and glass-ceramics. Therefore, it becomes highly important to understand the HCA formation and bone bonding mechanism as well as the rational design of better bone-forming biomaterials for the suitable applications.

Within the glass and glass-ceramic systems, 45S5 bioglass® ($0.224Na_2O{\cdot}0.269CaO{\cdot}0.026P_2O_5{\cdot}0.461SiO_2$) and other glass compositions close to this system represent an important group of bioactive material used for the scaffolds in the tissue engineering [7]. The reason behind this particular composition showing fast formation of HCA layer and mineralization is not completely understood in the literature. Increasing evidence in the literature indicates that ionic dissolution products from the various classes of materials are key to understand the behavior in vitro and in vivo, in the context of tissue engineering applications. More recently, it has been shown that bioactive glass dissolution products cause the rapid expression of several genes that regulate osteogenesis and the production of growth process [8]. Secondly, an ideal

scaffold material should combine the beneficial properties of bioactive glasses with a structure consisting of an interconnected network with macropores as well as the mesopores. Since, the macropores structure provides the potential for tissue ingrowths and the mesopores structure enables fast release of ionic products and enhances the bioactivity. In this direction, several methods have been developed for synthesis of bioactive glass and glass-ceramics such as conventional sol-gel route, flame synthesis, and freeze drying technique etc., however, each method has its own merits and demerits [9-11]. Among the various methods of preparation, the sol-gel method has led to tune the compositions in a wider range, an interconnected nanoporous structure and can be prepared under simpler conditions. More interestingly, the templated sol-gel glasses results in hierarchical structure in terms of surface area, surface morphology, void space, pore volume, and porosity than the conventional sol-gel derived glasses [12].

Mesoporous bioactive glasses (MBGs) have been synthesized during the last decade as an alternative approach to enhance the bioactivity [13] by using non-ionic surfactant as the structure directing agent and evaporation induced self assembly (EISA) process. In the previous chapter, we have shown that wormhole-like bioactive mesostructured sodium silicate glasses by acid assisted sol-gel method followed by EISA process using non-ionic block copolymer as structure directing agent [14]. Although, the rate of bioactivity-composition correlations are observed in melt derived bioactive glasses [15], the presence of reactive silanols have a dominating contribution to the superior in vitro bioactivity behavior in MBGs [16,17]. It is interesting to note from the different investigations that the superior textural properties such as high porosity facilitate rapid release of ions into the physiological fluids. This exchange process favors the Si-OH formation inducing nucleation and crystallization of apatite. Thus, the relation between enhanced bioactivity, composition and texture is still unclear owing to complicated interdependence between composition, pore size and surface area.

Despite many advantages of 45S5 glass and its close compositions as scaffold materials, still faces a technical complexity like high hydrolysis reactivity of sodium alkoxide precursors [18]. Due to this reason many researchers have turned to use alkaline-

earth containing glasses as bioactive materials, e.g., in vitro and in vivo studies have shown the enhanced bioactivity of Sr- and Mg-doped silicate/phosphate glasses [19, 20]. The main advantage of sodium containing glasses is that it shows the improved mechanical properties without losing a satisfactory biodegradability [18]. In this direction few attempts have been made to synthesis sodium containing ternary bioactive glasses but ended up with glass ceramics [21]. Within the ternary/quaternary system, an alternative protocol was adopted to prepare bioactive glasses but it has been found that the preparation of phosphosilicate glasses possible only with high phosphorus which acts as main glass-former [22]. Presence of high alkali oxide in the glass network significantly influence the ion exchange processes at the initial stage of Hench Mechanism (HM) of HCA layer formation, there by influencing the biological properties of the glass. It is widely accepted that the HM is responsible for the HCA layer formation in silicate-based bioactive glasses. The recent studies reveal that presence of both CaO and P_2O_5 in the glass system greatly enhances the bioactive behavior due to the formation of $Ca_3(PO_4)_2$ clusters (CaP), which provide natural nucleation sites for the further growth of HCA phases [23]. Hence, there must be different mechanism responsible for the superior bioactivity of hierarchically porous phosphorous containing BGs. Additionally, the coexistence of hydroxyapatite with highly soluble $NaCaPO_4$ phase was recently reported to have fast in vitro bioactivity [24].

In the present work, we report the apatite forming ability of different potentially important bioactive sol-gel prepared mesoporous silicate glasses and towards understanding the role of CaO and P_2O_5 in terms of the unique structures of MBG's. A comparative study of sol-gel derived ternary and quaternary MBG's revealed that later possesses a numerous features desirable in biomaterials used for the bone tissue engineering. We have obtained all the glasses by acid assisted sol-gel synthesis using non-ionic block copolymer followed by evaporation induced self assembly process under similar conditions. Obtained samples has been characterized in terms of structural and textural properties (change in surface area, pore size distribution and pore volume) followed by in vitro test in the simulated body fluid. We have found that the joint presence of calcium and phosphorous in the quaternary silicate glasses (Si-Na-Ca-P) accelerated growth rate of HCA formation than the

ternary glass system (Si-Na-P and Si-Na-Ca) where the similar textural properties yield poor HCA formation.

6.2 EXPERIMENTAL SECTION

6.2.1 Materials and Method

Mesoporous bioactive silicate glasses (MBGs) in the ternary and quaternary system with different chemical compositions as listed in Table 6.1 were prepared by means of acid assisted sol-gel route followed by EISA process. The following chemicals were used as precursors for synthesis of MBGs: Tetraethyl orthosilicate (TEOS) (Aldrich 99%), sodium acetate (NaAc) (Sigma Aldrich 99%), calcium acetate (CaAc), Triethylphosphate(TEP), Ethanol (AR, china),Acetic Acid, non-ionic amphiphilic triblock copolymer (P123) that has following sequence: $EO_{20}PO_{70}EO_{20}$, where EO is poly (ethylene oxide) and PO is poly(propylene oxide) (Aldrich) (M_w=5800), and Deionised water (DI). Briefly, the molar ratios of TEOS, TEP, NaAc and CaAc were designed according to molar ratio of SiO_2, Na_2O, CaO, P_2O_5 content. To achieve clear sol P123, TEOS,TEP, NaAc, CaAc and acetic acid were dissolved in ethanol after one hour interval and stirred at room temperature for 24 hrs and the corresponding molar ratio of TEOS/TEP: ethanol=1:4, TEOS/TEP: water=1:4 and weight ratio of water: acid=1:6. The resulting sol was then introduced into the petridish to undergo EISA process. Following this, as evaporated gel was aged for 3 days and then dried at 100 ^oC for 48 hrs. Additionally, we have adopted the acid treatment for template removal and calcinations at 400^oC for 4 hrs.

6.2.2 Characterization

The as prepared samples were characterized by WAXRD, SAXS, FTIR, and N_2-sorption techniques. The *in-vitro* bioactivity of as prepared samples was carried out immersing them in SBF with ionic concentration nearly equal to the human plasma at different intervals. An evolution of the SBF concentrations was monitored by means of pH value caused by the ion exchange processes between bioactive glass and the surrounding medium. Additionally, the surface morphology of soaked samples were characterized by XRD, FTIR, SEM, and N_2-SORPTION techniques to study the evolution of apatite layer.

6.3 RESULTS AND DISCUSSION

6.3.1. Structural, Morphological, and Textural Characterization

The wide angle X-ray diffraction (WAXRD) has been carried out on all MBGs and no sharp diffraction peaks appearing on the obtained XRD patterns except a broad reflection at $2\theta = 15^{o}$-35^{o}, which suggests that all MBGs with different chemical compositions found to be in amorphous state. The FTIR spectra of as prepared glass samples are dominated by the vibrational bands due to Si-O vibrational modes: Si-O-Si stretch, Si-O alkali stretch and Si-O bend and Si-O rock as shown in Figure 6.1. All the samples show very strong absorption peak at 1000-1200 cm^{-1}, assigned to Si-O-Si asymmetric stretching mode and the peaks at 800 cm^{-1} and 465 cm^{-1} are assigned to symmetric stretching and rocking vibration of Si-O-Si band. The observed peak around 970 cm^{-1} in all the compositions is assigned to non-bridging oxygen (NBO's) together with the surface silanols (Si-OH) groups which enhances the rate of apatite formation. Additionally, the surface silanol groups are confirmed by presence of a broad band in the region 3000-3770 cm^{-1}, which represents the vibration of different hydroxyl groups. This band is composed of the superposition of stretching modes of non-hydrogen-bonded silanols (isolated silanol groups) and hydrogen-bonded silanol (vicinal or germinal silanol groups) [16]. It is important to note that the band in the region 1000-1300 cm^{-1} is becoming narrower with an increase of CaO content in the quaternary glass system.

In addition to the above mentioned band assignments in the high frequency region, the following assignments can be made for the wave numbers below 1250 cm^{-1}. The IR vibrational bands of $(SiO_4)^{4-}$ and $(PO_4)^{3-}$ tetrahedral units occur in nearly identical spectral range 1200-1250 cm^{-1}, expect for the P=O stretching modes, exists in the orthophosphates. The band at 925 cm^{-1} is assigned to the Si-NBO stretching vibrations of three membered siloxane rings of SiO_4 units together with P-NBO stretching vibrations of PO_4 tetrahedral units. Based on the IR results, it is difficult to draw more conclusions about the quantification of various anionic units with the variation of CaO content. Thus, further investigations like site specific technique like NMR is highly necessary for a comprehensive understanding of the variation of different anionic groups and their composition dependence.

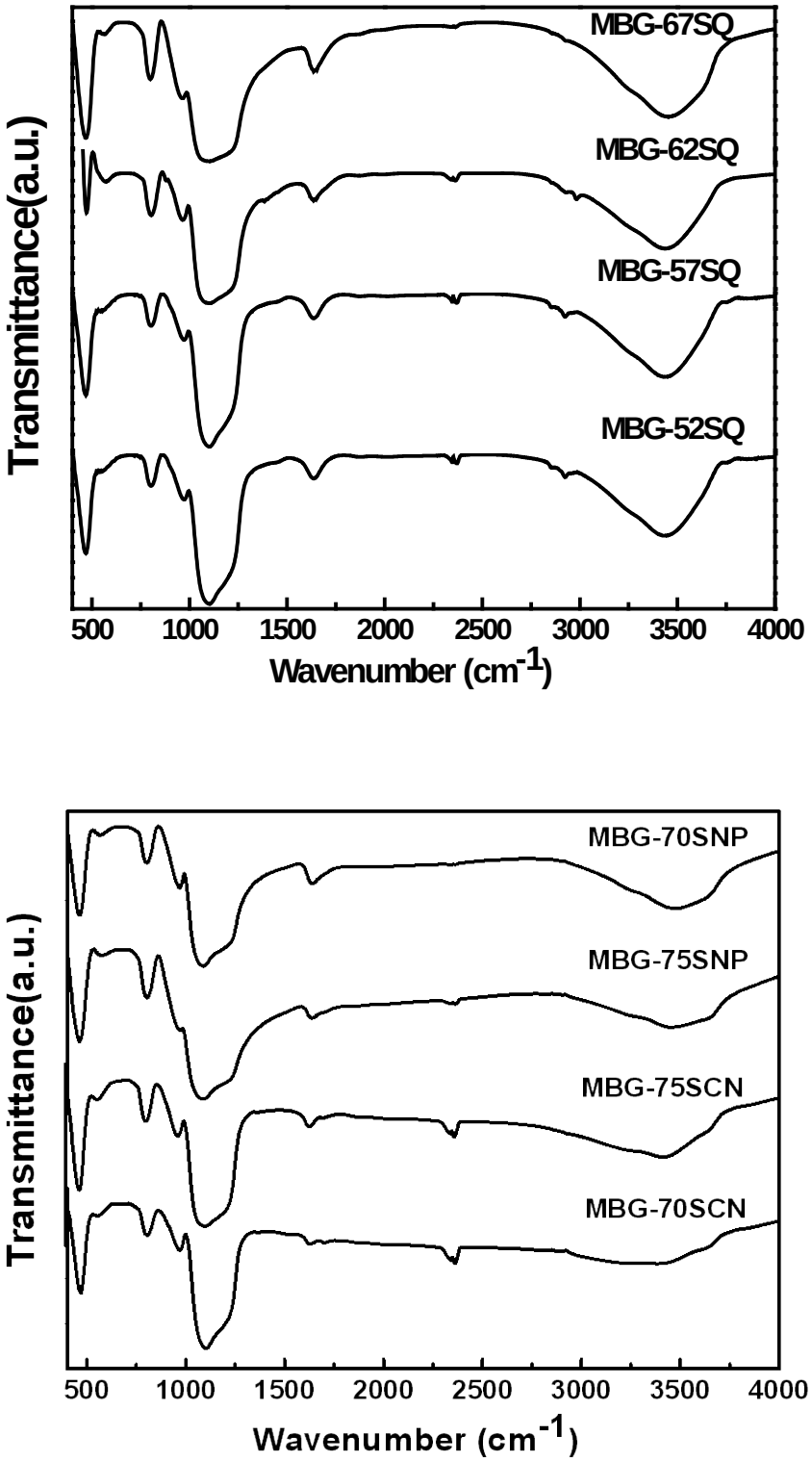

Figure 6.1: *FTIR Spectra of MBG-67SQ, MBG-62SQ, MBG-57SQ, MBG-52SQ MBG-75SNP, MBG-70SNP, MBG-75SNC AND MBG-70SNC glasses before soaking in SBF.*

However, the IR spectrum of ternary glasses shows the marked differences in high and low frequency regions as compared to the quaternary glasses. It is worthwhile to note that the asymmetric stretching peak is broader in the samples containing phosphorus (MBG-67SQ, 57SQ, 75SNP) and the reason being the presence of phosphate vibrational modes at 1140 cm^{-1}(Si-O-P) and 1037 cm^{-1}(P-O) which are overshadowed by the strong Si-O-Si vibrational mode at 1000-1300 cm^{-1}[17]. Moreover, absorption peak at 1630 cm^{-1} is attributed to surface adsorbed water and hydroxyl groups (silanol groups) on the sol-gel glasses, which can accommodate more water molecules owing to the large surface area and high porosity.

The vibrational band at 1630 cm^{-1} and the broad band at 3000-3770 cm^{-1} are more prominent in the case of glasses containing phosphorus due to the presence of more surface silanol groups. The band around 560-600 cm^{-1} corresponds to bending vibration of P-O bonds, which are visible only in the Si-Na-P system and suggest that phosphate enters as network former. On the other hand, in the case of CaO containing ternary glasses, the band at 840-750 cm^{-1} shows the broad spectrum reflecting the Si-O-Si symmetric stretching vibrations and the network modifier character of Ca^{2+} ions [18].

The arrangement of mesopores structure can be clearly seen in the HRTEM images. The images obtained on the as prepared samples depict a wormhole-like mesoporous structure similar to previous work on mesoporous sodium silicate glasses [5]. Glasses show large number of channels with short range packing, but lacking discernible long-range packing order. With an increase of alkaline-earth content the mesoporous structure tend to become more disordered confirming collapse of the framework structure caused by the disruption of Si-O-Si network [19]. Nitrogen adsorption-desorption isotherm of all the quaternary and ternary compositions exhibits a type IV isotherm typical of a mesoporous structure. The obtained textural properties of the investigated samples are listed in Table 6.1.

Table 6.1: *Chemical composition and textural parameters.*

Sample	Nominal composition (mol%)	Surface area (m^2g^{-1})	Pore volume (ccg^{-1})	Pore diameter (nm)
MBG-67SQ	$67.4SiO_2$-$25Na_2O$-5CaO-$2.6P_2O_5$	308.6	1.46	34.9
MBG-62SQ	$62.4SiO_2$-$25Na_2O$-10CaO-$2.6P_2O_5$	253.3	1.34	30.6
MBG-57SQ	$57.4SiO_2$-$25Na_2O$-15CaO-$2.6P_2O_5$	226.9	1.54	24.8
MBG-52SQ	$52.4SiO_2$-$25Na_2O$-20CaO-$2.6P_2O_5$	209.3	1.68	21.7
MBG-75SNP	$75SiO_2$-$20Na_2O$-$5P_2O_5$	556.5	1.06	8.1
MBG-70SNP	$70SiO_2$-$20Na_2O$-$10P_2O_5$	648.2	0.99	3.5
MBG-75SNC	$75SiO_2$-$20Na_2O$-5CaO	291.3	1.55	15.1
MBG-70SNC	$70SiO_2$-$20Na_2O$-10 CaO	359.3	1.49	13.3

In Figure 6.2 to 6.4, we illustrate the nitrogen adsorption isotherms and pore size distribution curves (inset) for quaternary and ternary MBG in the present investigation. It has been observed that although all the samples own similar type IV isotherm typical of mesoporous material but it shows different hysteresis loop: MBG-67SQ, MBG-57SQ, MBG-70SNC and MBG-75SNC exhibit H1 type hysteresis loops (corresponding to cylindrical pores) whereas MBG-75SNP possess H2 type loop corresponding to the ink bottle type pores [19]. High phosphorous content in MBG-70SNP glass leads to change in the shape of hysteresis loop of H4 type, associated with narrow slit-like pore structure [20]. It is interesting to note that the capillary condensation pressure i.e. the P/P_0 value at which desorption branch meets adsorption branch is different in all the compositions reflecting the variation in the pore sizes. On the other hand, in the case of ternary Si-Na-P system surface area has increased significantly at the expense of decrease in pore diameter. This can be due to addition of P_2O_5 in the sodium silicate glass structure as network former evidenced by the P-O-Si linkage from the FTIR measurements. Thus, the increased network connectivity in glass structure leads to the enhanced textural properties with the addition of P_2O_5 content [21].

Apparently, all the samples show narrow pore size distribution (as seen in inset) and their distribution were determined using BJH model from the adsorption branch. Based on the obtained textural properties, we have found that higher pore diameter and surface area greatly enhance the apatite formation in these glasses.

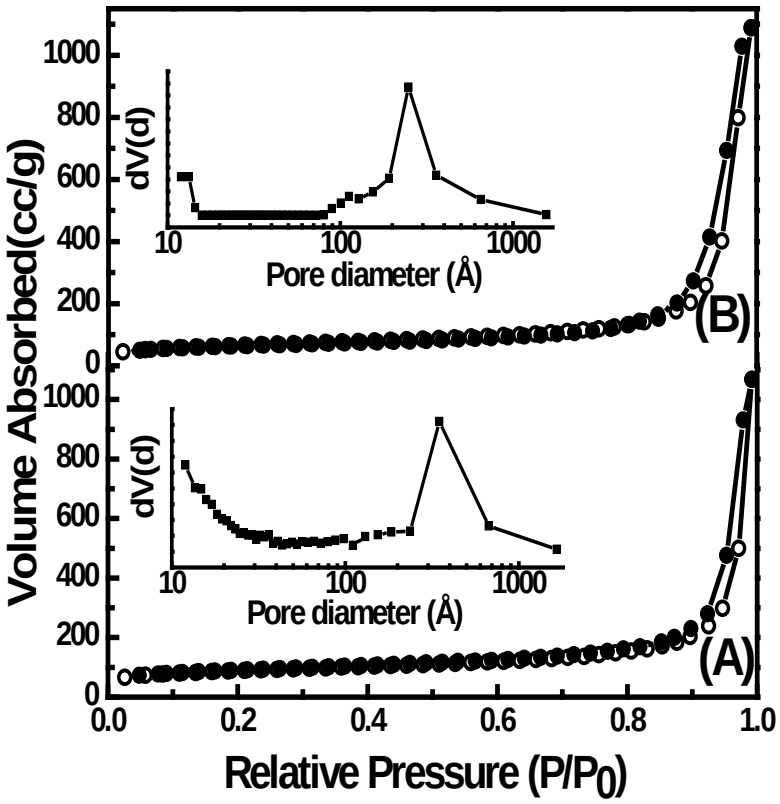

Figure 6.2: *Nitrogen adsorption-desorption isotherm and pore size distribution (inset) of (A) MBG- 67SQ (B) MBG-57SQ glasses.*

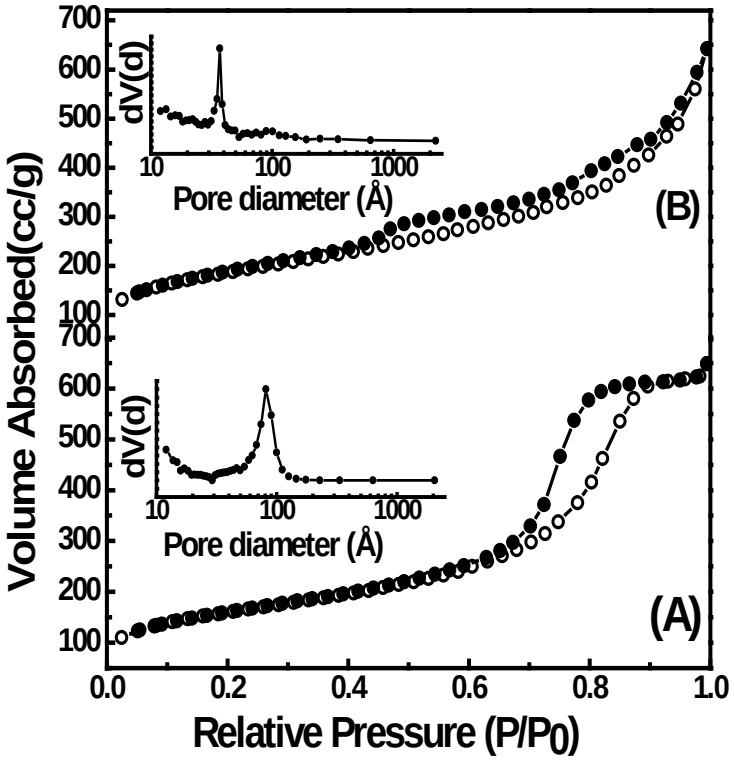

Figure 6.3: *Nitrogen adsorption-desorption isotherm and pore size distribution (inset) of (A) MBG-75SNP (B) MBG-70SNP glasses.*

In addition, mesoporosity will promote bioresorption of the materials such as proteins and growth factors without the loss of biologic functions [22]. It is clearly evident that variation of the textural properties with composition clearly indicates that the local structure of MBG's plays an important role.

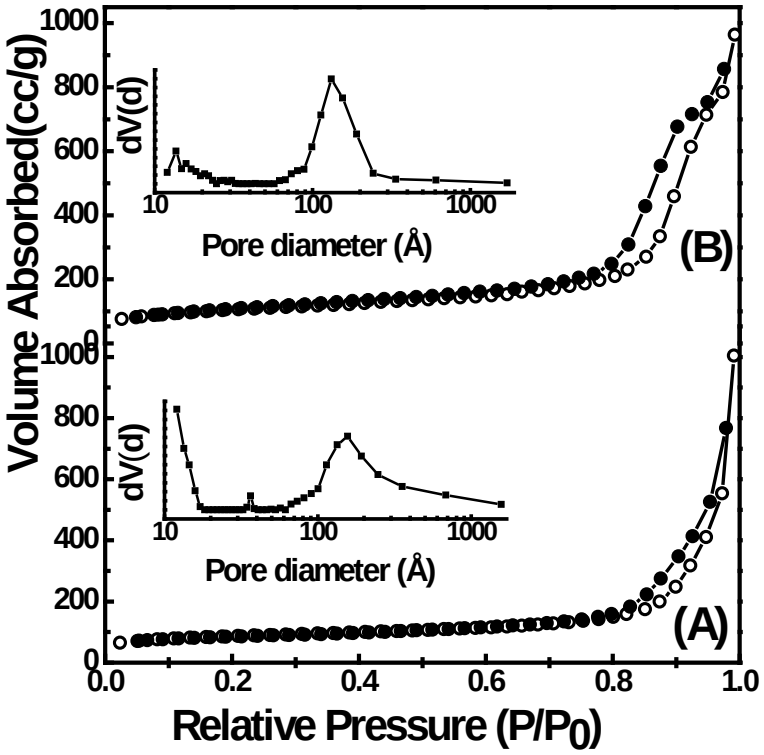

Figure 6.4: *Nitrogen adsorption-desorption isotherm and pore size distribution (inset) of (A) MBG-75SNC (B) MBG-70SNC glasses.*

6.3.2. In Vitro Bioactivity Test

The pH values of the SBF solution after immersing the as prepared samples for 12h, 1D and 3D are shown in Figure 6.5. The sharp rise in the pH values with time is due to strong ion exchange processes on the glass surface. Cations such as Na^+ and Ca^{2+} near the glass surface get exchanged for H^+ or H_3O^+ from the solutions, which raise the pH value of the SBF solution [23]. The P-bearing glasses showed a steep rise in pH values from 7.40 to 7.8 within first 12h of immersion in SBF whereas in P-free samples (MBG-70SCN) the pH rise was less pronounced (from 7.4 to 7.7).

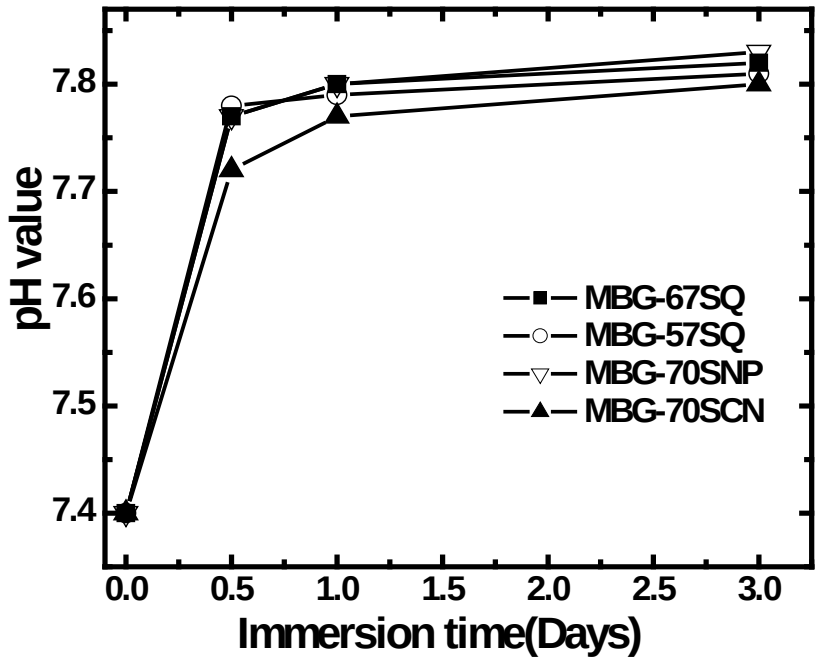

Figure 6.5: *The variation of pH values of the SBF with soaking time on different MBG's.*

After the initial pH increase, it remains almost constant over for 3 days of the immersion. The initial rise in pH is due the first stage of HM, i.e., the diffusion controlled process which leads to hydrolysis of silica group creating silanols after rapid ion exchange. The high surface area and silanol density of the quaternary and ternary glass system studied eases the ion exchange favoring pH rise. Thereafter, a continuous silanol formation at the glass interface and then condensations as well as the reploymerization of SiO2-rich layer on the surface exhaust alkali and alkaline-earth cations. Subsequently, the pH of the solution remains constant due to the rapid growth of apatite phase that overcome the release rate of ions into the solution [24]. Therefore, the resulting pH depends on buffering capacity of surrounding solution, surface area and composition of the immersed glass [25].

WAXRD pattern of samples soaked in SBF for different time durations are shown in Figures 6.6 and 6.7. Clearly, after immersion of the glass samples in SBF for different intervals, we observe an appreciable change in the diffraction pattern.

On comparing the XRD pattern of phosphorus bearing (P-bearing) and phosphorous free (P-free) glass compositions, it has been observed that P- bearing quaternary system (Figures 6.6A and 6.6B) exhibits sharp Braggs reflections that

corresponds to an apatite-like phase within 12 h of immersion in SBF (JCPDS number 09-0432). Additionally, it is interesting to note that the glasses with high surface area show fast crystallization of formed amorphous HCA layer than the glasses with high amount of CaO content. These results reveal that the crystallization of amorphous HCA is strongly influenced by the textural properties.

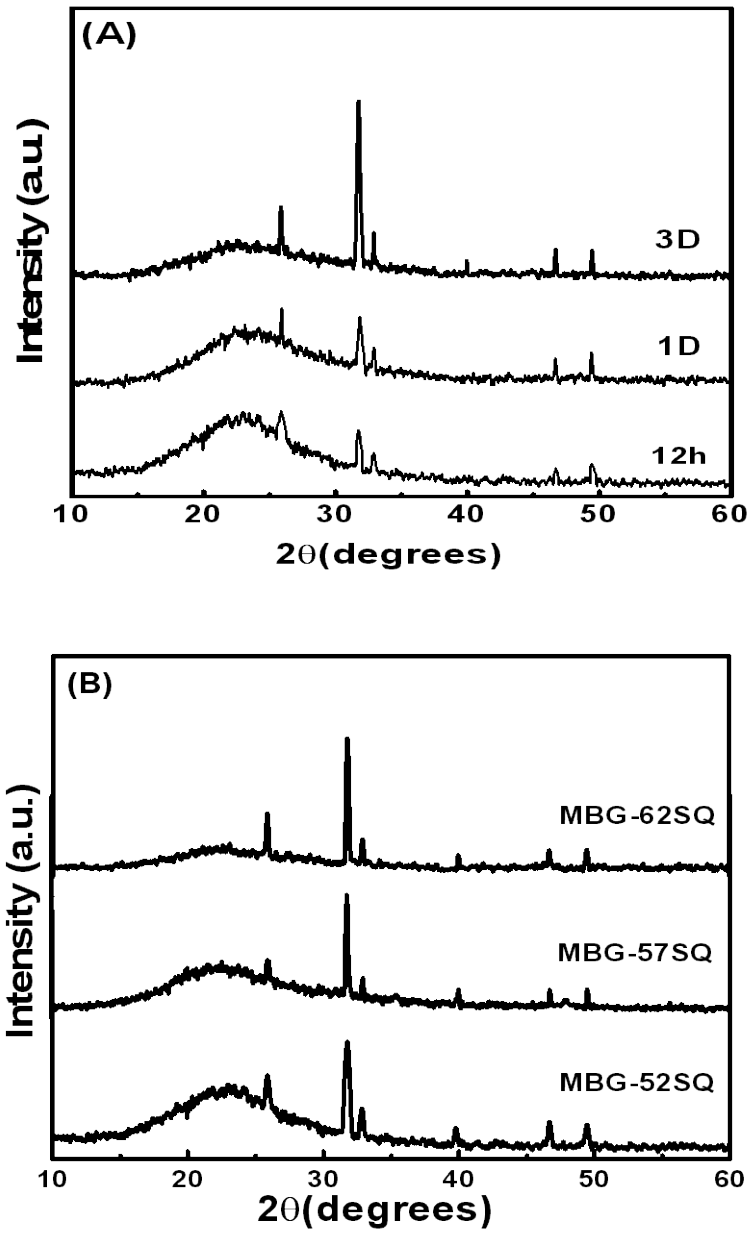

Figure 6.6: *XRD pattern of (A) MBG-67SQ glass after soaking in SBF for 12h, 1D and 3D (B) MBG-62SQ, MBG-57SQ, and MBG-52SQ glass after soaking in SBF for 3D.*

In contrast to the quaternary glasses, the P-bearing ternary system (MBG-75SNP and MBG-70SNP) (Figures 6.7A and 6.7B) shows only slight maxima corresponding to (002) and (211) apatite reflections after 12 h soaking in SBF. On comparing three days soaking of P-bearing glasses, XRD pattern shows the intense reflections on MBG-70SNP compared to MBG-75SNP which could be attributed to the large surface area. However, the obtained XRD pattern clearly shows on these two samples (P-bearing) that the formed apatite phase co-exists in amorphous and crystalline forms with nearly equal amount. In the case of P-free samples (Figures 6.7C and 6.7D), the formation of apatite becomes very poor and it remains mainly in amorphous form even after long hour exposure in the SBF solution.

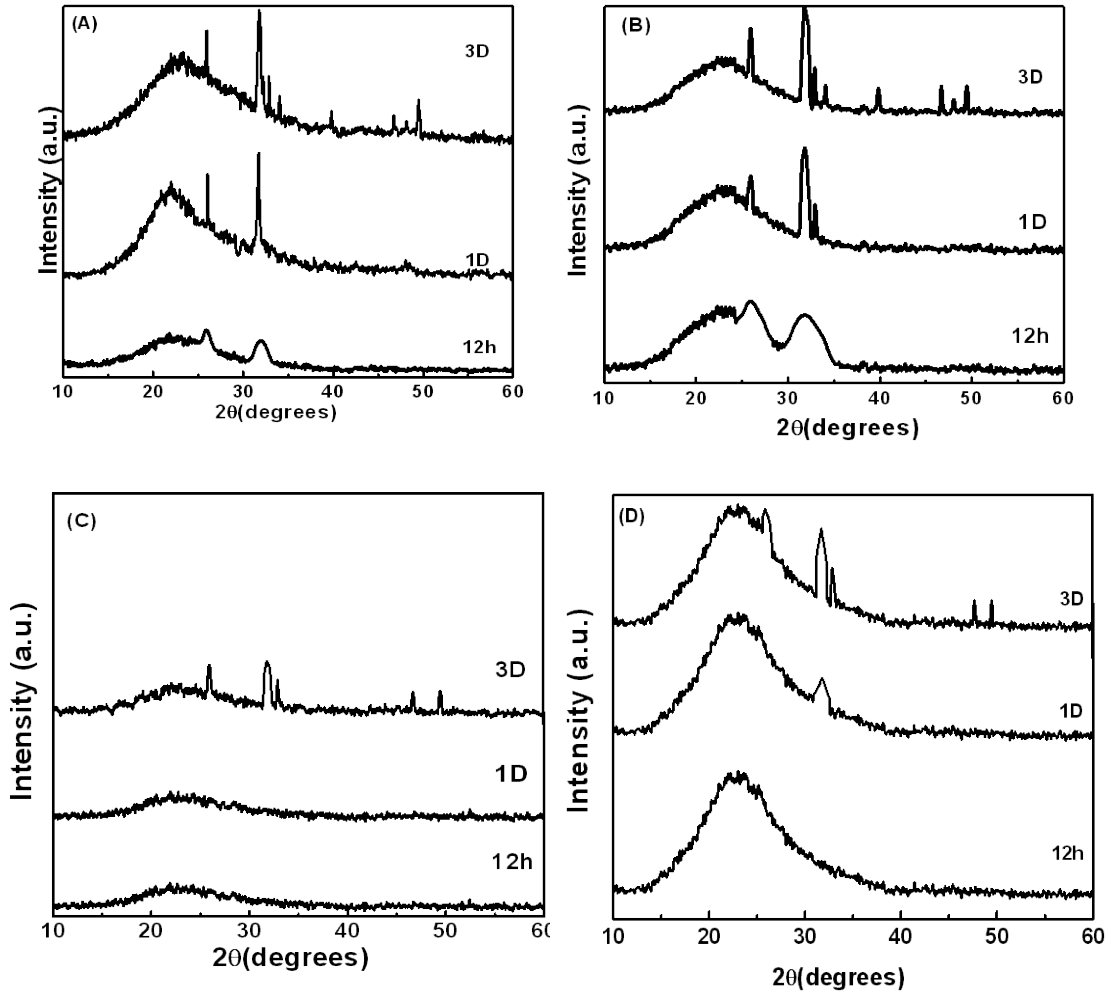

Figure 6.7: *XRD pattern of (A) MBG-70SNP (B) MBG-75SNP (C) MBG-75SNC (D) MBG-70SNC after soaking in SBF for 12h, 1D and 3D.*

Therefore, P-free compositions show significantly lower rate of apatite formation than P-bearing compositions in addition to the lack of crystallanity in the formed apatite layer. Based on these results, we suggest that both the surface area as well as the composition of the glasses play a significant role in the formation and mineralization of apatite.

The quaternary glasses have both calcium as well as phosphorous which results in the faster formation of calcium phosphate (CaP) clusters on the pore wall of silica and results in the easy formation of nucleating sites of HCA [26-28]. Although MBG-75SNP and MBG-70SNP have high surface area but the rate of apatite crystallization is slower than quaternary system which could be due to absence of CaP clusters. Thus, XRD results provide unambiguously the influence of texture and composition on the formation of apatite and subsequent mineralization.

Furthermore, it is very early to comment on the nucleation and crystallization of apatite phase on the nanoscale level with the currently available data. In this context, we have observed that the presence of sodium rich orthophosphate glasses favor the increased rate of apatite deposition on the glass surface by XRD results and in agreement with earlier NMR studies [29-31]. However, the crystallization of apatite rich phase is hindered by other kinetic parameters, which could be compensated with the presence of CaO. It is known that this phase is extremely soluble and effectively increase the actual content of phosphorus into super saturation in the external physiological environment in the biological implants. By comparing these three different systems, P-free ternary composition show least apatite formation than P- bearing ternary and quaternary compositions since the sodium silicate species has low solubility as well as the poor textural properties [29]. Secondly, in the case of P-free compositions, the Ca^{2+} cation is distributed within the silica network, which makes the cation difficult to be accessible to SBF.

The SBF soaked samples are further characterized by the FTIR as shown in Figure 6.8. The characteristic vibrational modes originates from the silicate glass network decreases in intensity and the bands due to HCA layer become dominant upon exposure to the SBF. The spectra of P-bearing quaternary system (MBG-67SQ and MBG-62SQ) after 12h, 1D and 3D of incubation time show the significant difference from the virgin sample spectra's. More specifically, the weak P-O vibrational bands near 562, 603, 960

cm^{-1} indicating initial presence of poor crystalline CaP-rich layer together with the bands of the carbonate groups at 876, 1422 and 1480 cm^{-1} [32]. Additionally, the spectra reveals the disappearance of 960 cm^{-1} band and a shift of 1090 cm^{-1} corresponding to Si-O-Si stretching modes towards the lower wave number of 1045 cm^{-1} corresponding to P-O stretching mode with increasing soaking time, which indicates the formation of apatite rich layer on the glass surface [33]. On the other hand, in the case of MBG-70SNP glass sample single band was observed at 560 cm^{-1} after 1D soaking in the SBF as shown in Figure 6.8(C).

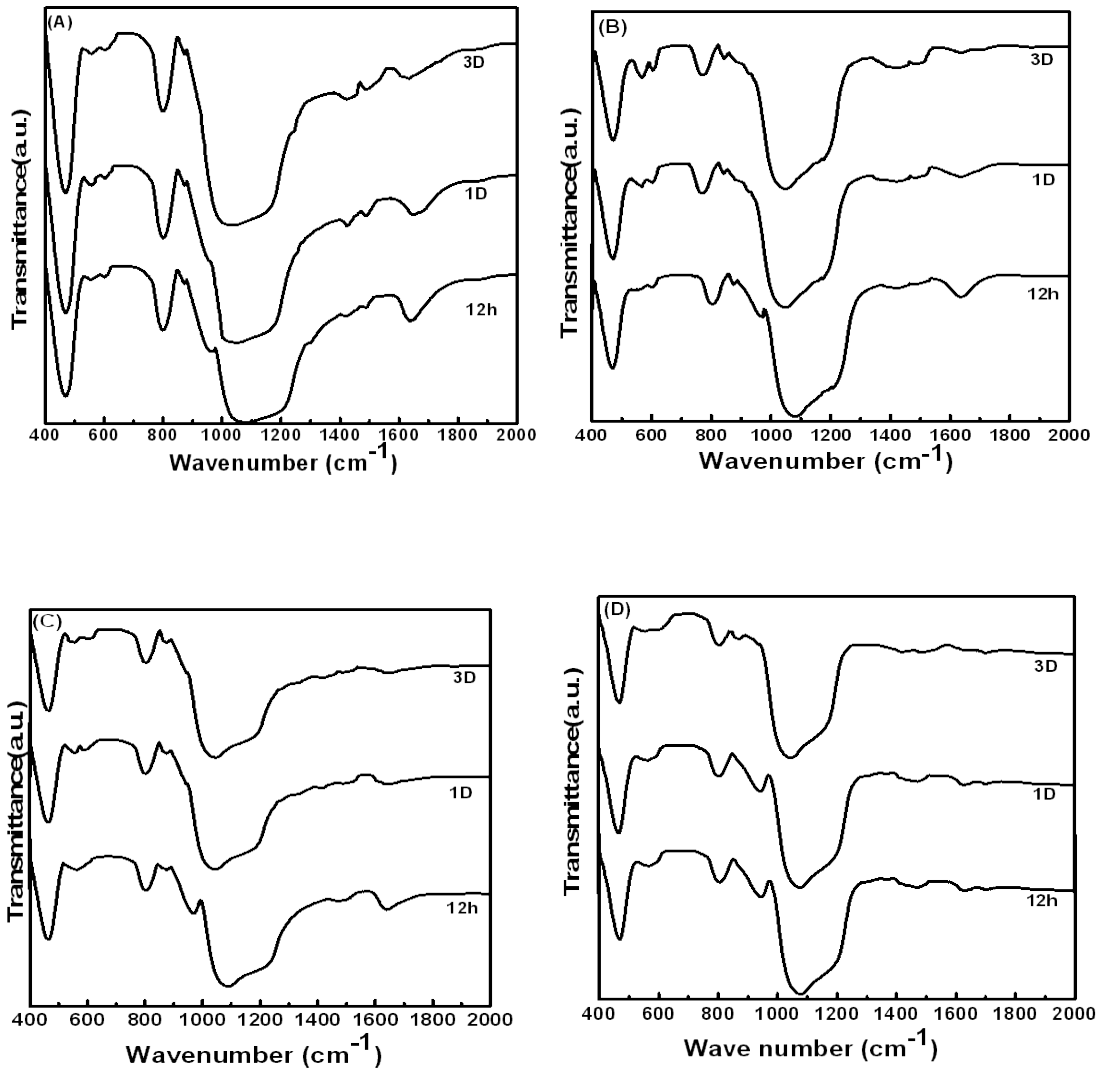

Figure 6.8: *FTIR Spectra of (A) MBG-67SQ (B) MBG-62SQ (C) MBG-70SNP (D) MBG-70SNC glasses as a function of soaking time in SBF for 12h, 1D and 3D.*

This single broad band reveals the presence of apatite precursor on the glass surface and it further splitting into 556 and 603 cm^{-1} band with an increase in soaking duration substantiate the crystalline rich apatite formation [34]. In case of P-free glasses, the weak phosphate and carbonate vibrational bands has been observed even after three days of soaking time evidence the formation of deprived crystalline apatite layer [35]. It is possible that the faster rate of apatite formation in P-bearing compositions could be explained by the dual phase pore wall model [27].

Within this model, it was found that P-bearing MBGs broadly consists of two components (i) silica rich $CaO\text{-}SiO_2$ pore wall and (ii) a minor amorphous calcium orthophosphate components which incorporates water molecules as well as OH^- ions and contributes to superior bioactivity observed from MBGs by in vitro studies. Therefore, the apatite formation from MBGs can be controlled by several parameters such as composition of glass, textural property and the concentration of silanol groups present on the glass surfaces. However, in case of P-free MBGs the concentration of silanols is the crucial factor [28]. It has been observed that P-free MBGs having same textural parameters as P-bearing glass show the poor apatite formation [26]. Therefore, we suggest that the bioactivity of MBGs is not only influenced either by high surface area or high concentration of silanols but also the presence of CaP clusters on the pore walls which acts as nucleation sites as well as increasing the rate of apatite deposition on glass surface [36].

In Figures 6.9 and 6.10, we report SEM micrographs of MBG-67SQ, MBG-57SQ, MBG-70SNP and MBG-70SNC glasses with different interval of soaking in SBF. The surface of MBG-67SQ (Figure 6.9A) and MBG-57SQ (Figure 6.9B) (P-bearing quaternary glasses) appears to be relatively smooth before soaking in SBF. After 12h immersion in SBF, the elongated particles of irregular shapes appear which implies the degradation of samples in such a short time. On the other hand, the longer exposure in SBF (three days immersion), a small spherical as well as quasi-spherical particles were observed and distributed homogenously over the glass surface.

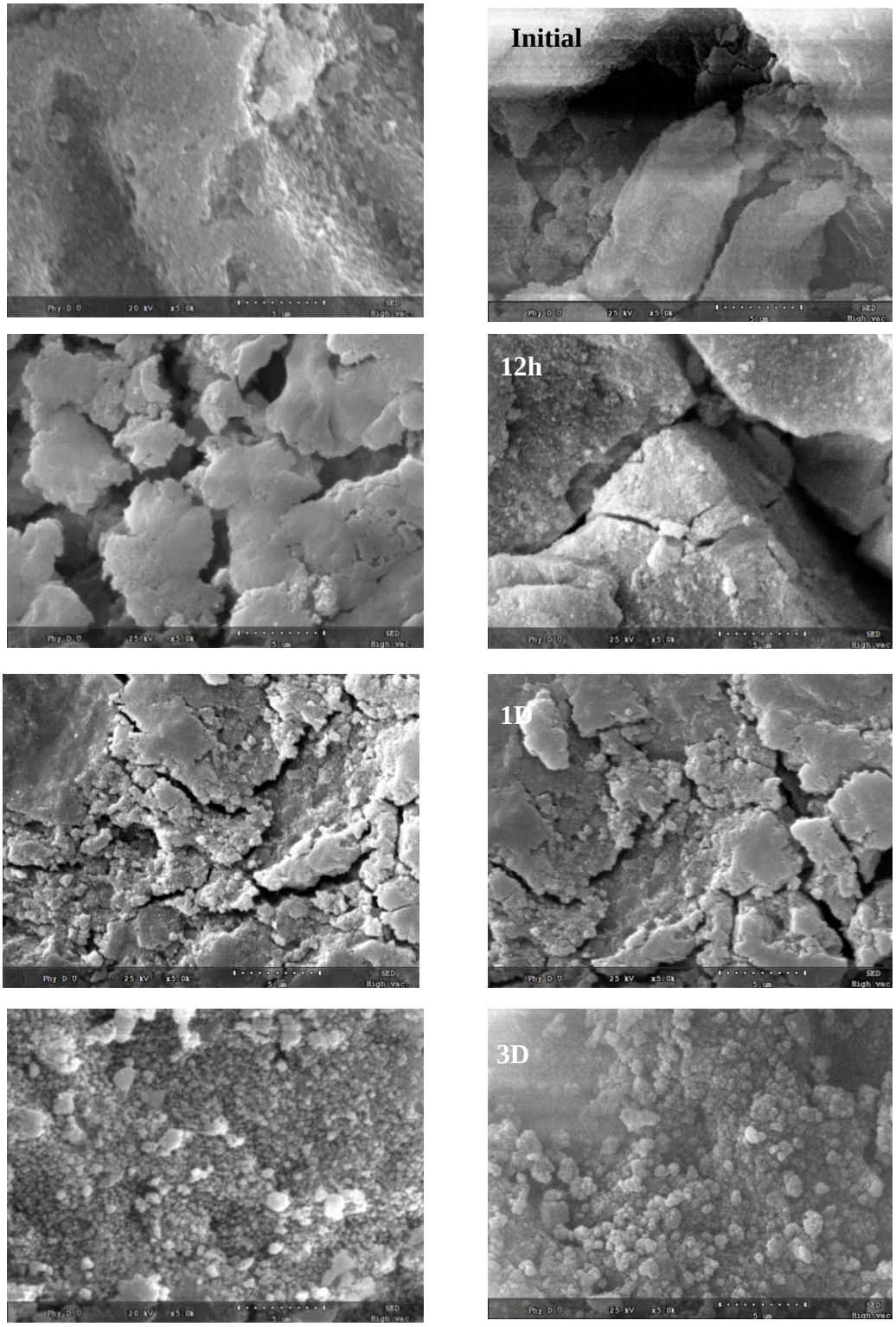

Figure 6.9: SEM micrographs of (A) MBG-67SQ (B) MBG-62SQ glasses before and after soaking in SBF for 12h, 1D and 3D.

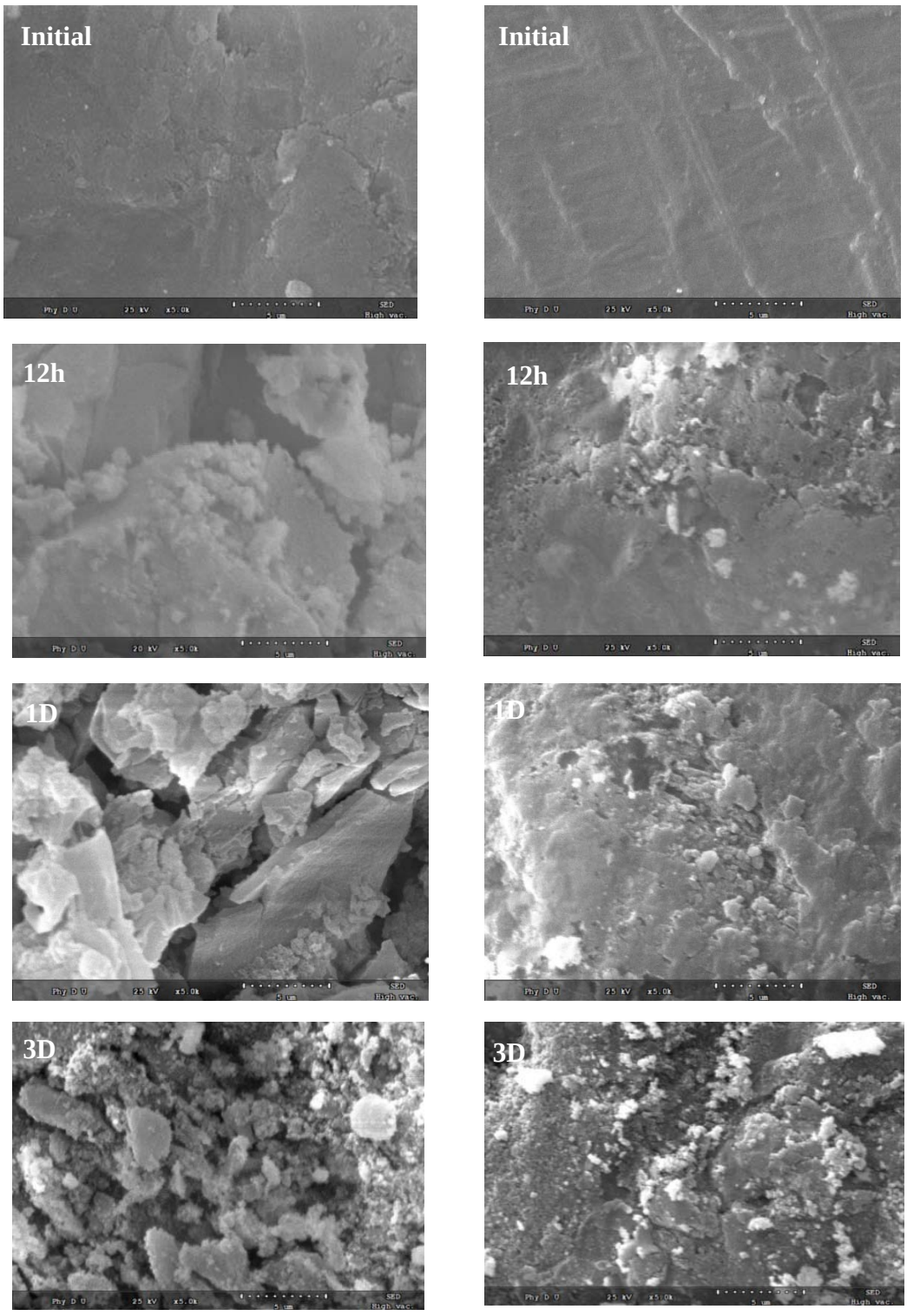

Figure 6.10: *SEM micrographs of (A) MBG-70SNP (B) MBG-70SNC glasses before and after soaking in SBF for 12h, 1D and 3D.*

Thus, the presence of phosphate and calcium in the glass system favors nucleation and growth of CaP domains as proposed earlier investigations for the apatite formation [37, 38]. As seen from the FTIR spectra (Fig 6.8) after 12h soaking period of MBG-70SNP glass sample reveals singlet around 560 cm^{-1} assigned to amorphous CaP. In the case of MBG-67SQ glass, a doublet at 556 and 603 cm^{-1} characteristic of crystalline CaP due to the presence of small CaP crystallites. Additionally, the cross-sectional SEM observations on these SBF soaked samples reveals that the high surface area sample enhances the faster and substantially thick amorphous CaP formation without crystallization. It is interesting to note that the surface of MBG-70SNP (Figure 6.10A) glass covered with appreciable amount of spherical particles. The SEM micrographs of MBG-70SNC before and after soaking in SBF reveal that the glass surface remains same as shown in Figure 6.10B. Thus, the SEM results further support the WAXRD and FTIR observations that the high silanol density, superior textural properties and appropriate composition (presence of calcium and phosphorus together) are the key factors responsible for high in vitro bioactivity of MBGs [1].

Nitrogen adsorption/desorption isotherms and pore size distribution curves of representative MBG's after immersion in SBF solution for 3D are shown in Figure 6.11. It can be seen that the nitrogen adsorption-desorption isotherm curves of MBG's (Figures 6.11A, 6.11B and 6.11D) are identified as type IV isotherms with H1 type hysteresis loop whereas MBG-70SNP (Figure 6.11C) exhibits H4 type hysteresis loop. However, the relative pressure at which hysteresis and capillary condensation occurs is different from the virgin glass samples.

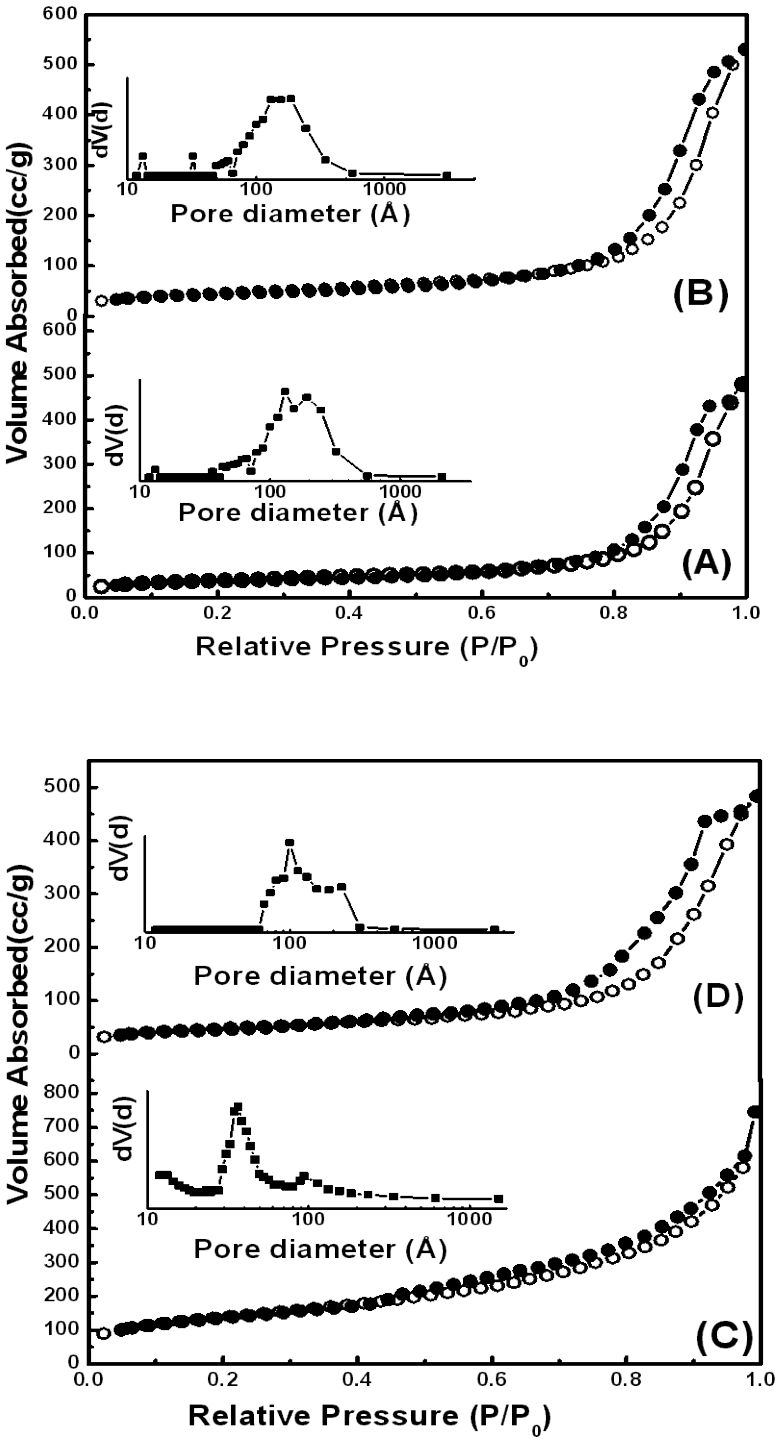

Figure 6.11: *Nitrogen adsorption-desorption isotherm and pore size distribution (inset) of (A) MBG-67SQ (B) MBG-57SQ (C) MBG-70SNP (D) MBG-70SNC glasses after soaking in SBF for 3 days.*

Additionally, we present the obtained results of BET surface area, pore volume and BJH pore diameter after immersion in SBF for three days are listed in Table 6.2.

Table 6.2: *Textural parameters of samples after soaking in SBF for 3 days.*

Sample	Surface area (m^2g^{-1})	Pore volume (ccg^{-1})	Pore diameter (nm)
MBG-67SQ	209.6	1.46	Bimodal 12.8-19.2
MBG-57SQ	162.4	0.82	Broadening 11.1-24.4
MBG-70SNP	493.4	1.15	Bimodal 3.6-9.3
MBG-70SNC	267.9	1.09	Bimodal 12.6-18.5

The surface area of the virgin glass samples decreases to some extent after soaking in SBF, which is due to the HCA phase formation in the mesoporous channels. The pore size distribution curves show broadening and presence of bimodal pores after soaking in SBF. Within the bimodal pore size distribution, smaller pore dimension are same as before soaking which suggest that some pores are retained even after soaking. The larger pore sizes might be due to occurrence of interconnected mesoporous channels resulting from various ions release during soaking period [6] or may be due to the hydration of Si-O-Si and P-O-P bonds in the glass network which facilitates apatite formation [39]. The changes in the BET surface area are apparent from the Table 6.2 that the samples MBG-70SNP endure greater variation in the surface area than MBG-67SQ.

6.4 CONCLUSIONS

In this study, we have investigated the role of calcium and phosphorus on structural, morphological, textural properties and invitro bioactive behavior in sodium oxide containing mesoporous Si-Ca-Na-P quaternary and ternary Si-Na-P as well as Si-Ca-Na glass systems. The results obtained by various analytical techniques reveals that

the presence of orthophosphate in the glass system greatly influences the structural, morphological and textural properties. These changes are directly correlated with the apatite forming ability or so called “Bioactivity” of the mesoporous glass system. It has been observed that presence of phosphorus and calcium promotes the apatite mineralization. The dual-phase pore wall model provides the understanding of the excellent in-vitro bioactivity of P-bearing quaternary system in comparison with P-bearing and P-free ternary system. Additionally, we find that the high surface area, pore volume and uniform pore size distribution related to high amount of Si-OH groups, will account for the variation in bioactivities between P-bearing and P-free mesoporous samples. Due to large concentration of silanol groups in these mesoporous glasses, accelerate the first three-stages of the Hench mechanism and results the amorphous CaP (ACP) clusters. These observations indicate that chemical composition, textural properties and the presence of accessible ACP clusters determine the invitro bioactive behavior.

REFERENCES

[1] I. Izquierdo-barba , M. Vallet-Regi, Solid State Sciences 13 (2011) 773-783.

[2] T. Kokubo, H. Kushitani, S. Sakka, T. Kitsugi, T. Yamamuro, J. Biomed. Mater. Res. 24 (1990) 721-734.

[3] M.M. Pereira, A.E. Clark , L.L. Hench, J.Am. Ceram. Soc. 78 (1995)1769-1774.

[4] M.M. Pereira, L.L.Hench, J. Sol-Gel. Sci. Technol. 7 (1996) 59-68.

[5] C. Vaid, S. Murugavel, R. Khashyap, R.P. Tandon, Micro. Meso. Mater. 159 (2012)17-23.

[6] X.X. Yan, H.X. Deng, X.H. Huang, G.Q. Lu, S.Z. Qiao, D.Y.Zhao, C.Z. Yu , . Non-Cryst. Solids 51 (2003) 3209–3217.

[7] A.J. Salinas, A.I. Martin, M. Vallet-Regi, J. Biomed. Mater. Res. 61(2002)524- 532.

[8] M.Vallet-Regi, I. Izquierdo-barba , A.J. Salinas, J. Biomed. Mater. Res. 46(1999) 560-565.

[9] M. Vallet-Regi, A.J. Salinas, J. Ramirez-Castellanos, J.M. Gonzalez-Calbet, Chem.Mater. 17(2005)1874-1879.

[10] Q.Z. Chen, Y. Li, L.Y. Jin, J.M.W. Quinn, P.A. Komesaroff , Acta. Biomater. 6 (2010) 4143-4153.

[11] E. Gentleman, Y. Fredholm, G. Jell, N. Lotfibakhshaiesh, M.D. O'Donnell, R.G. Hill, M.M. Stevens, Biomaterials 31 (2010) 3949–3956.

[12] I. Ahmed ,A. Parsons, A. Jones, G. Walker, C. Scotchford, C. Rudd, J Biomater Appl 24 (2010) 555–575.

[13] R.L. Siqueira, O. Peitl, E.D. Zanotto, Mater. Sci. Eng. C 31(2011) 983-991.

[14] D. Carta, D.M. Pickup, J.C. Knowles, M.E. Smith, R.J. Newport, J. Mater. Chem. 15(2005)2134-2140.

[15] J. Andersson, S. Areva, B. Spliethoff, M. Mika Linde´n, Biomaterials 26(2005)6827– 6835.

[16] H. Aguiar, J. Serra, P. Gonzalez, B. Leon, 355, (2009) 475-480.

[17] A. Aronne et. al. Chem. Mater. 17(2005) 2081-2090.

[18] A. Meiszterics, L. Rosta , H. Peterlik, J. Rohonczy, S. Kubuki, P. Henits , K. Sinko, J.Phys. Chem. A 114(2010)10403-10411.

[19] T. Xiu, Q. Liu, J. Wang 16(2006)4022-4024.

[20] K.S.W. Sing, D.H. Everett, R.A.W. Haul, L. Moscou, R.A. Pierotti, J. Rouquerol, T. Siemieniewska Pure & Appl. Chem. 57(1986) 603-619.

[21] A.J. Salinas, A.I. Martin, M. Vallet-Regi, J. Biomed. Mater. Res. 61(2002)524- 532.

[22] Y. Zhu, C. Wu, Y. Ramaswamy, E. Kockrick, S. Paul, S. Kaskel, H. Zreiqat, Micropor. Mesopor. Mater. 112(2008)494-503.

[23] P. Horcajada, A. Ramila, K. Boulahya, J. Gonzalez-Calbet, M. Vallet-Regi , Solid State Sci. 6(2004)1295-1300.

[24] A.Martinez, I. Izquierdo-barba, M. Vallet-Regi, 12(2000)3080-3088.

[25] M.Q.Du etal, Am. J. Dent. 21(2008) 210-214.

[26] A. Garcia, M. Cicuendez, I. Izquierdo-Barba, D. Acros, M.Vallet-Regi, Chem. Mater. 21(2009)5474-5484.

[27] E. Leonova, I. Izquierdo-barba, D. Acros, A. Lopez-Noriega, N. Hedin, M. Vallet- Regi, M. Eden , J. Phys. Chem. C 112(2008)5552-5562.

[28] P.N. Gunawidjaja etal , J. Phys. Chem. C 114(2010)19345-19356.

[29] M.W.G. Lockyer, D.Holland, R. Dupree, J. Non-Cryst. Solids 188(1995)207-219.

[30] H. Gruaaaute, L. Montagne, G. Palavit, J.L. Bernard, J. Non- Cryst. Solids 263(2000)312-317.

[31] M.D. O'Donnell, S.J. Watts, R.V. Law, R.G. Hill, J. Non-Cryst. Solids 354 (2008) 3554-3560.

[32] I. Notingher, J.R. Jones, S. Verrier, I. Bisson, P. Embanga, P. Edwards, J.M. Polak Spectroscopy 17(2003)275-288.

[33] M. Mneimne, R.G. Hill, A.J. Bushby, D.S. Brauer, Acta. Biomater. 7(2011)1827-1834.

[34] D.S. Brauer, N. Karpukhina, M.D. O'Donnell, R.V. Law, R.G. Hill, Acta. Biomater. 6(2010)3275-3282.

[35] M.D. O'Donnell, S.J. Watt, R.G. Hill, R.V. Law, J. Mater. Sci: Mater. Med. 20(2009)1611-1618.

[36] D. Jagadeesan, C. Deepak, K. Siva, M.S. Inamdar, M. Eswaramoorthy, J. Phys. Chem. C 112(2008)7379-7384.

[37] M. Vallet-Regi, I.Izquierdo-barba, A.J. Salinas, J. Biomed. Mater. Res. 46 (1999)560-565.

[38] M. Vallet-Regi, A.J. Salinas, M. Gil, J. Mater. Chem. 9(1999)515-518.

[39] S. Zhao, Y. Li, D. Li, Micropor. Mesopor. Mater. 135(2010)67-73.